Article

Estimation of Potato Above-Ground Biomass Using UAV-Based Hyperspectral images and Machine-Learning Regression

Yang Liu [1,2,3,†], Haikuan Feng [1,4,*,†], Jibo Yue [5], Yiguang Fan [1], Xiuliang Jin [6], Yu Zhao [1], Xiaoyu Song [1], Huiling Long [1] and Guijun Yang [1]

1 Key Laboratory of Quantitative Remote Sensing in Agriculture of Ministry of Agriculture and Rural Affairs, Information Technology Research Center, Beijing Academy of Agriculture and Forestry Sciences, Beijing 100097, China
2 Key Lab of Smart Agriculture System, Ministry of Education, China Agricultural University, Beijing 100083, China
3 Key Laboratory of Agricultural Information Acquisition Technology, Ministry of Agriculture and Rural Affairs, China Agricultural University, Beijing 100083, China
4 College of Agriculture, Nanjing Agricultural University, Nanjing 210095, China
5 College of Information and Management Science, Henan Agricultural University, Zhengzhou 450002, China
6 Institute of Crop Sciences, Chinese Academy of Agricultural Sciences/Key Laboratory of Crop Physiology and Ecology, Ministry of Agriculture, Beijing 100081, China
* Correspondence: fenghk@nercita.org.cn
† These authors contributed equally to this work.

Abstract: Above-ground biomass (AGB) is an important indicator for monitoring crop growth and plays a vital role in guiding agricultural management, so it must be determined rapidly and nondestructively. The present study investigated the extraction from UAV hyperspectral images of multiple variables, including canopy original spectra (COS), first-derivative spectra (FDS), vegetation indices (VIs), and crop height (CH) to estimate the potato AGB via the machine-learning methods of support vector machine (SVM), random forest (RF), and Gaussian process regression (GPR). High-density point clouds were combined with three-dimensional spatial information from ground control points by using structures from motion technology to generate a digital surface model (DSM) of the test field, following which CH was extracted based on the DSM. Feature bands in sensitive spectral regions of COS and FDS were automatically identified by using a Gaussian process regression-band analysis tool that analyzed the correlation of the COS and FDS with the AGB in each growth period. In addition, the 16 Vis were separately analyzed for correlation with the AGB of each growth period to identify highly correlated Vis and excluded highly autocorrelated variables. The three machine-learning methods were used to estimate the potato AGB at each growth period and their results were compared separately based on the COS, FDS, VIs, and combinations thereof with CH. The results showed that (i) the correlations of COS, FDS, and VIs with AGB all gradually improved when going from the tuber-formation stage to the tuber-growth stage and thereafter deteriorated. The VIs were most strongly correlated with the AGB, followed by FDS, and then by COS. (ii) The CH extracted from the DSM was consistent with the measured CH. (iii) For each growth stage, the accuracy of the AGB estimates produced by a given machine-learning method depended on the combination of model variables used (VIs, FDS, COS, and CH). (iv) For any given set of model variables, GPR produced the best AGB estimates in each growth period, followed by RF, and finally by SVM. (v) The most accurate AGB estimate was achieved in the tuber-growth stage and was produced by combining spectral information and CH and applying the GPR method. The results of this study thus reveal that UAV hyperspectral images can be used to extract CH and crop-canopy spectral information, which can be used with GPR to accurately estimate potato AGB and thereby accurately monitor crop growth.

Keywords: potato; canopy original spectra; first-derivative spectra; vegetation indices; plant height; support vector machine; random forest; Gaussian process regression

1. Introduction

Potatoes are the fourth largest food crop in the world after wheat, corn, and rice. It is an important crop for national food security given its ability to adapt to its environment, its ease of cultivation, its short production cycle, and its high yield, so research on potatoes is particularly important [1–3]. Timely and accurate information on potato crop growth is vital for supporting agricultural production management and for macroregulation of cropping patterns and excavating production potential [4–7].

Above-ground biomass (AGB) is an important physiological indicator and is closely related to the nutritional status of crops and the ability of stems and leaves to accumulate organic matter, so it is often used to monitor crop growth [8–11]. Traditionally, AGB is measured by field-sampling surveys, which not only consume significant time and energy but also damage crops. In addition, the method is inefficient due to the limitation of sampling points because it can only be applied to small areas and thus cannot be scaled up to monitor crops grown in large areas [12,13].

Ground objects reflect and absorb electromagnetic waves, which sensors can remotely detect. Through data processing and comprehensive analysis, the characteristics of ground objects can thus be monitored remotely [14]. In recent years, remote-sensing technology has been used to dynamically estimate physiological and biochemical crop indicators to monitor crop growth. This continuous observation allows for nondestructive acquisition of crop-canopy spectral information [15–17]. In particular, remote sensing by using unmanned aerial vehicles (UAVs) has proven mobile, flexible, easy to implement, and produces high-resolution images. This approach has thus rapidly developed for acquiring small-scale regional crop phenotype information to monitor growth [18–21]. In contrast with the digital and multispectral sensors often carried by UAV platforms, hyperspectral sensors detect in narrow spectral bands that cover a broad spectrum. Subtle differences in ground objects may thus be distinguished by deep mining of the hyperspectral data. Based on the multilevel and multi-angle analysis of the hyperspectral characteristics of a crop canopy, an AGB estimation model may be developed to study the real-time dynamic change in AGB, which allows crop growth to be monitored [22–25]. Therefore, UAV hyperspectral remote-sensing technology is gaining attention in precision agriculture as a way to rapidly obtain accurate crop information.

Currently, the estimation of crop AGB using visible–near-infrared remote-sensing techniques is mainly done by using physical and statistical models. The physical models are based on the radiative transfer mechanism and require numerous parameters (meteorological data, soil data, crop variety information, etc.) as input to simulate crop growth and finally estimate the AGB. For example, physiological development time, soil data, temperature data, and vegetation indices (VIs) have been used to estimate maize AGB [26,27]. Although the physical model has a strong potential for generalization, it is mechanistically complex and requires numerous experimental supports in practical applications. It is also limited by its input parameters, which makes it difficult to apply on a large scale [28–32]. The statistical models are based on the relationship between crop-canopy spectral information and AGB. An AGB estimation model is constructed from spectral feature parameters, VIs, or regression techniques, which are simple in form, efficient in operation, and widely adaptable for monitoring crop growth. For example, a continuous projection algorithm was used to extract eight sensitive spectral bands (706, 724, 734, 806, 808, 810, 812, and 816 nm) to estimate winter wheat AGB [33]. Based on the optimal VIs, AGB estimation models were constructed to monitor the growth of rice [8], maize [11], and winter wheat [34]. Winter wheat AGB was accurately estimated by combining different VIs with partial-least-squares regression (PLSR) [35], stepwise regression (SWR) [36], and multiple linear regression (MLR) [23], respectively. Other studies estimate AGB by applying several regression techniques simultaneously, using correlation analysis to confirm sensitive spectral parameters, and then building an AGB estimation model through PLSR and MLR. They report that the PLSR-AGB model is more stable and consistent than the MLR-AGB model [37].

Most reports establish the correlation between crop AGB and VIs by traditional regression techniques. In fact, the estimations of crop AGB over multiple growth periods using VIs formed from visible–near-infrared spectra are limited due to the canopy spectral saturation caused by the growth stages effect [38]. However, although crop height (CH) that has been extracted based on the structure-from-motion technique combined with canopy spectral information can inhibit canopy saturation and allow for more comprehensive AGB estimation in multiple growth periods [39–41], few studies have been used to monitor variations in potato AGB. In recent years, machine-learning methods combined with remote-sensing data have been more commonly used to monitor AGB [42,43]. The machine-learning methods include random forest (RF) and support-vector machine (SVM) and are increasingly used to estimate crop AGB. In addition, Gaussian process regression (GPR) is gradually gaining importance for monitoring crop AGB because it has fewer input parameters, is better able to deal with nonlinearities using kernel functions, and solves the black-box problem in the machine-learning regression process [44,45]. Heretofore, no studies have extracted CH information and canopy spectral information from UAV hyperspectral images and fed these data to machine-learning methods to explore the accuracy of AGB estimation models over the various potato growth stages.

The main objectives of this study thus include (1) verifying the reliability of potato CH data that have been extracted by using a digital surface model (DSM) generated by the structure-from-motion technique; (2) comparing the accuracy of AGB estimates for different potato growth stages made by the GPR, RF, and SVM methods fed with (a) spectral data and (b) spectral data and CH; and (3) exploring the use of machine-learning regression to quantify the AGB based on UAV remote-sensing data.

2. Materials and Methods

2.1. Study Area Location and Experimental Design

The study area was in the National Precision Agriculture Research and Demonstration Base in Xiaotangshan Town, Changping District, Beijing, China, which is located at 40°10′34″ N, 116°26′39″ E.

A planting-density test area, a nitrogen test area, and a potassium-fertilizer test area were set up in the trial field, and two early-maturing potato varieties, Zhongshu 5 (Z5) and Zhongshu 3 (Z3), were selected to increase the spatial variability of crop growth in the field. The planting-density test area was planted in three densities: 60,000(P1), 72,000(P2), and 84,000 (P3) tubers/ha, and 18 test plots were treated six times with three replications. The nitrogen test area was treated at four levels: 0 (N0), 112.5 (N1), 225 (N2), and 337.5 (N3) kg/ha pure N, and 24 test plots were treated eight times with three replications. The potassium-fertilizer test area was treated at three levels: 0 (K0), 495 (the planting-density and nitrogen test areas were treated this way), and 990 (K2) kg/ha KO_2, and six test plots were treated twice with three replications. All plots were treated with 90 kg/ha P_2O_5. The plots totaled 48, and each had a sample area of 6.5 m × 5 m. To accurately locate the test plots of the split-plot experiment, 11 ground control points were evenly distributed around the test plots for terrain correction. The specific experimental design is shown in Figure 1.
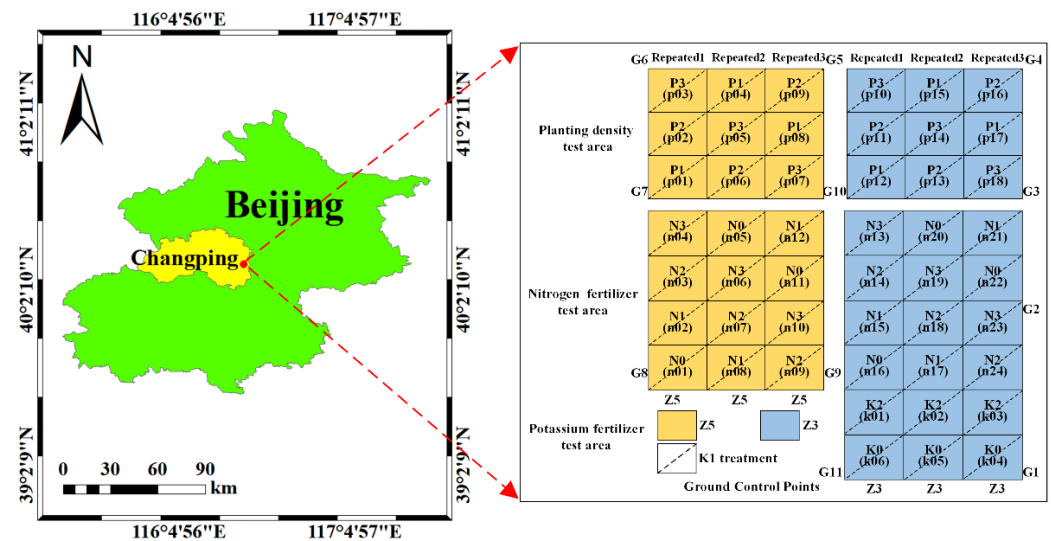
Figure 1. Location and design of test area.

2.2. Ground Data Acquisition and Processing

We obtained the AGB and CH for the potato tuber-formation stage (28 May 2019, BBCH-41), tuber-growth stage (10 June 2019, BBCH-44), and starch-storage stage (20 June 2019, BBCH-47). (1) AGB data acquisition: To ensure that reasonable samples were acquired, three plants representative of the overall growth level were destructively sampled from each plot and immediately sealed in plastic bags and transported to the laboratory. After separating stem from leaf, they were washed with running water, put into an oven at 105 °C for 1 h, then held at 80 °C to dry for over 48 h until the mass was constant. The dry mass of the stems and leaves was determined by using a high-precision balance (accuracy 0.001 g) and summed to obtain the dry mass of the sample. Finally, the potato AGB of each plot was obtained based on the population density and sample dry mass. (2) CH data acquisition: Four representative plants were selected from each plot and the distance from the bottom of the stem to the tip of the top leaf was measured with a straightedge. The average of four such measurements was taken as the potato CH of the plot.

2.3. Acquisition and Processing of UAV Hyperspectral Remote-Sensing Data

This experiment used a six-rotor electric UAV (M600, SZ DJI Technology Co., Ltd., Shenzhen, Guangdong, China) equipped with a UHD185 Firefly imaging spectrometer (Cubert, Germany), with dimensions of 195 mm × 67 mm × 60 mm, a mass of 470 g, a spectral range of 450–950 nm, and a spectral resolution of 4 nm with 125 spectral channels. The imaging speed was one hyperspectral image cubes per second. To ensure the accuracy of the resulting DSM, the takeoff position was the same each time and the flight was undertaken at 12:00 PM when the sky was clear and without wind or clouds. In addition, the same flight route was used for each growth stage. The flight altitude was set to 20 m (the transect width was 6 m) and had a speed of about 1.5 m/s. The overlap of heading and side direction was set to 85%. Before each flight, black and white plate data were collected on the ground for radiometric calibrations. The UAV carried sensors to acquire hyperspectral images of the bare-soil stage (April 20), tuber-formation stage, tuber-growth stage, and starch-storage stage. The spatial resolution of the resulting images was 1.3 cm.

Once the images were acquired, they were preprocessed in two steps: (1) The first step was stitching and geometric correction of the UAV hyperspectral images. The grayscale images within the selected aerial zone were stitched together with Agisoft PhotoScan software (version 1.1.6; Agisoft LLC, St. Petersburg, Russia) by using the position information of the ground control points (the correction error in each period was less than 2 cm). Next, using Cuber-Pilot software (Germany), the hyperspectral images were fused with the grayscale images to form new hyperspectral images. Finally, the digital orthophoto map and DSM

of the test area were generated by using Agisoft PhotoScan software. (2) The second step involved extracting the canopy reflectance of the plot. The maximum-area vectors of different plots were plotted by using ArcGIS software (version 10.2; Esri, Redlands, CA, USA), the vector data were numbered by plot, and the average spectral reflectance of each area of interest was extracted by using the interactive data language implemented in ENVI software (version 5.0; Boulder, CO, USA). The result was used as the spectral reflectance of the potato canopy of the different plots.

2.4. Selection of Vegetation Indices

Vis are closely related to the physiological and biochemical parameters of crops and are often used to monitor crop growth. Therefore, we selected 16 commonly used Vis for estimating potato AGB. Table 1 lists the parameters and their mathematical expressions.

Table 1. Vis used in this study.

Vegetation indices	Equation	Reference
OSAVI (optimizing soil-adjusted vegetation index)	$1.16 \times (R800 - R670)/(R800 + R670 + 0.16)$	[46]
MTVI2 (modified triangular vegetation index 2)	$1.5 \times (1.2 \times (R800 - R500) - 2.5 \times (R670 - R550)) / (2 \times (R800 + 1)2 - (6 \times R800 - 5 \times (R670)1/2) - 0.5)^{1/2}$	[10]
SAVI (soil-adjusted vegetation index)	$(1 + 0.5) \times (R800 - R670)/(R800 + R670 + 0.5)$	[8]
RVI (ratio vegetation index)	$R810/R660$	[10]
NDVI (normalized-difference vegetation index)	$(R800 - R680)/(R800 + R680)$	[10]
EVI (enhanced vegetation index)	$2.5 \times (R800 - R670)/(R800 + 6 \times R670 - 7.5 \times R450 + 1)$	[47]
MCARI (modified chlorophyll-absorption ratio index)	$((R700 - R670) - 0.2 \times (R700 - R550))(R700/R670)$	[36]
RDVI (renormalized-difference vegetation index)	$(R800 - R670)/(R800 + R670)^{1/2}$	[36]
SPVI (spectral-polygon vegetation index)	$0.4 \times [3.7 \times (R800 - R670) - 1.2 \times |R550 - R670|]$	[36]
GNDVI (green normalized-difference vegetation index)	$(R750 - R550)/(R750 + R550)$	[48]
CI1 (red-edge chlorophyll index 1)	$R800/R740 - 1$	[49]
MSR (modified simple ratio index)	$(R800/R670 - 1)/(R800/R670 + 1)^{1/2}$	[48]
SIPI (structure-insensitive pigment index)	$(R800 - R450)/(R800 + R680)$	[50]
VARI (visible atmospherically resistance index)	$(R555 - R680)/(R555 + R680 - R480)$	[51]
NGRDI (normalized green–red difference index)	$(R560 - R680)/(R560 + R680)$	[42]
TVI (triangular vegetation index)	$0.5 \times [120 \times (R750 - R550) - 200 \times (R670 - R550)]$	[52]

2.5. Analysis Methods

RF is a method of data classification and statistical regression first proposed by Breiman and Cutler [53]. The method forms a training dataset by bootstrap sampling, generating random decision trees based on the classifier integrated into the system, then combining multiple decision trees to predict the dependent variable, and, finally, deciding the prediction results by voting. SVM is a class of generalized linear classifiers that perform binary classification of data by supervised learning. SVM are mainly classified as linear or nonlinear vector machines [42]. The training dataset is binary-classified by a kernel function to minimize the distance of all samples from a hyperplane and then the sample data are fit for prediction purposes [54]. GPR is a nonparametric probabilistic statistical model based on Bayes' theorem that learns the relationship between independent variables (e.g., spectral features) and dependent variables (e.g., AGB) by using mean and covariance functions based on maximum-likelihood estimation method. Compared with conventional machine-learning methods, parameter optimization is simpler and more suitable for training with small sample data, and the greatest advantage is the automatic identification of the best spectral features through the Gaussian process regression-band analysis tool (GPR-BAT) [45,55]. For sample training and prediction, this study uses the machine-learning regression algorithm of the ARTMO software (version 3.3.0; The University of Valencia, Spain, Europe).

2.6. Statistical Analysis

Forty-eight datasets were obtained for each fertility period. The data of the repeat 2 and repeat 3 plots were selected as the modeling set, and the data of the repeat 1 plots were used as the validation set. The detailed statistics are shown in Table 2. To reduce overfitting and underfitting, a tenfold cross-validation approach was used to construct the AGB estimation model for potatoes at different growth periods. The coefficient of determination (R^2), root–mean–square error of prediction (RMSE), and normalized root–mean–squared error (NRMSE) were used to assess the model fit and stability.

Table 2. Descriptive statistics for AGB (kg/hm^2) and CH (cm) of calibration and validation datasets.

Dataset	Crop Parameters	Min	Mean	Max	Standard Deviation	Coefficient of Variation (%)
Calibration	AGB	307	1144	2897	493	43.17
	CH	15.12	28.68	40.87	5.69	20.66
Validation	AGB	608	1281	2268	405	31.67
	CH	15.75	27.55	37.25	4.56	15.92

3. Results and Analysis

3.1. Extraction of Potato Crop Height

By using the raster calculation tool in the ArcGIS software, (i) the DSM of the potato tuber-formation, the tuber-growth, and the starch-storage stages and (ii) the DSM of bare-soil stage were calculated by difference, respectively. This gave the spatial distribution of CH for each growth period. Finally, the average CH of potatoes in each plot was extracted by using the area-of-interest tool. A total of 144 sets of average CH data were extracted for the three growth periods. To verify the reliability of based DSM extraction CH, the extracted CH and the measured CH were linearly fit (Figure 2). Figure 2 shows that the extracted CH with the measured CH fits better (R^2 = 0.84, RMSE = 2.52 cm, NRMSE = 9.05%), indicating that the extracted CH is reliable.
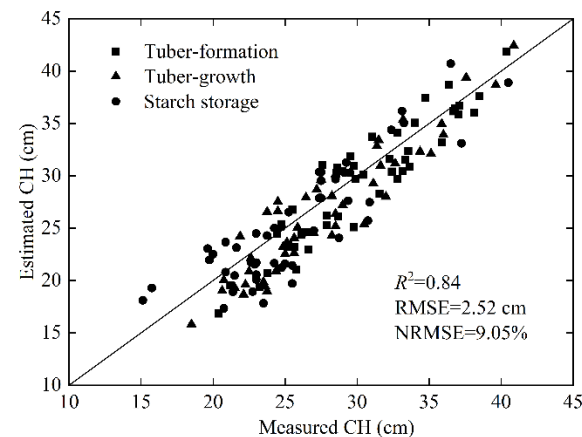

Figure 2. Measured and estimated potato CH.

3.2. Potato AGB Estimates Based on Canopy Spectra

In addition to the Vis formed by the common combination of bands, spectral feature parameters can also be formed from transformations such as spectral differentiation. First-order differentiation gives the change in reflectance, that is, the slope of spectral intensity with respect to wavelength. Hyperspectral data are suitable for first-order differentiation because of the high number of bands they contain. Figure 3 shows the correlation between (i) the canopy original spectra (COS) and first-derivative spectra (FDS) and (ii) the potato AGB at different growth stages. During the tuber-formation stage, the COS correlates significantly with the AGB in the near-infrared region (754–950 nm; $p < 0.01$), as does the FDS in both the red-edge (682–750 nm) and near-infrared regions. During the tuber-growth

stage, the COS correlates significantly with the AGB from the visible to the near-infrared ($r > 0.53$, $p < 0.01$), whereas the FDS correlates significantly with the AGB mainly in the green (502–598 nm), red-edge, and near-infrared regions. During the starch-storage stage, the COS correlates significantly with the AGB over the whole band ($r > 0.53$, $p < 0.01$), whereas the FDS correlates significantly with the AGB in the red (602–678 nm), red-edge, and near-infrared regions.
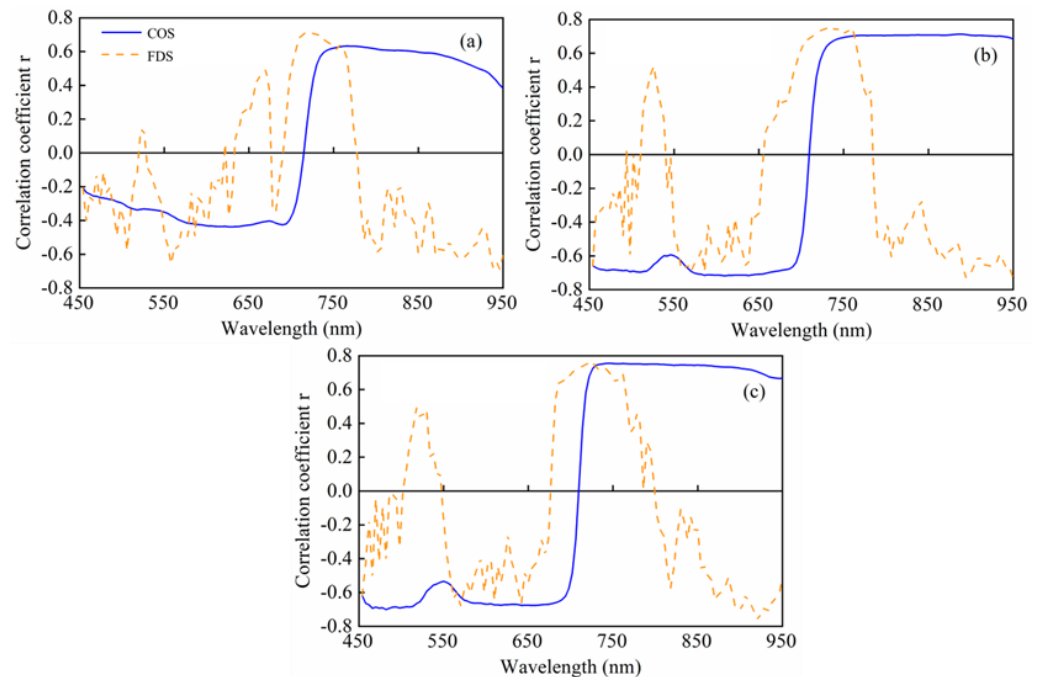

Figure 3. Correlation of canopy original spectra (COS) and first-derivative spectra (FDS) with above-ground biomass (AGB) of potatoes at different growth stages: (**a**) tuber-formation stage, (**b**) tuber-growth stage, (**c**) starch-storage stage.

The GPR-BAT was used to automatically identify spectral features in sensitive regions of the COS and FDS of the potato tuber-formation stage, tuber-growth stage, and starch-storage stage. A tenfold cross-validation was used in the GPR-BAT program. Figure 4 shows the mean RMSEcv, standard deviation, and min–max extreme value range of AGB estimated for each growth period by using the GPR method. Based on these results, the GPR-BAT determined that the optimal number of COS features for the tuber-formation, tuber-growth, and starch-storage stages were three (Figure 4a), six (Figure 4b), and four (Figure 4c), respectively. Likewise, the optimal number of FDS features were six (Figure 4d), seven (Figure 4e), and 11 (Figure 4f), respectively. The optimal COS and FDS features selected for each growth period were used to estimate potato AGB (Table 3).

Table 3. COS and FDS features selected by GPR-BAT for the tuber-formation, tuber-growth, and starch-storage periods.

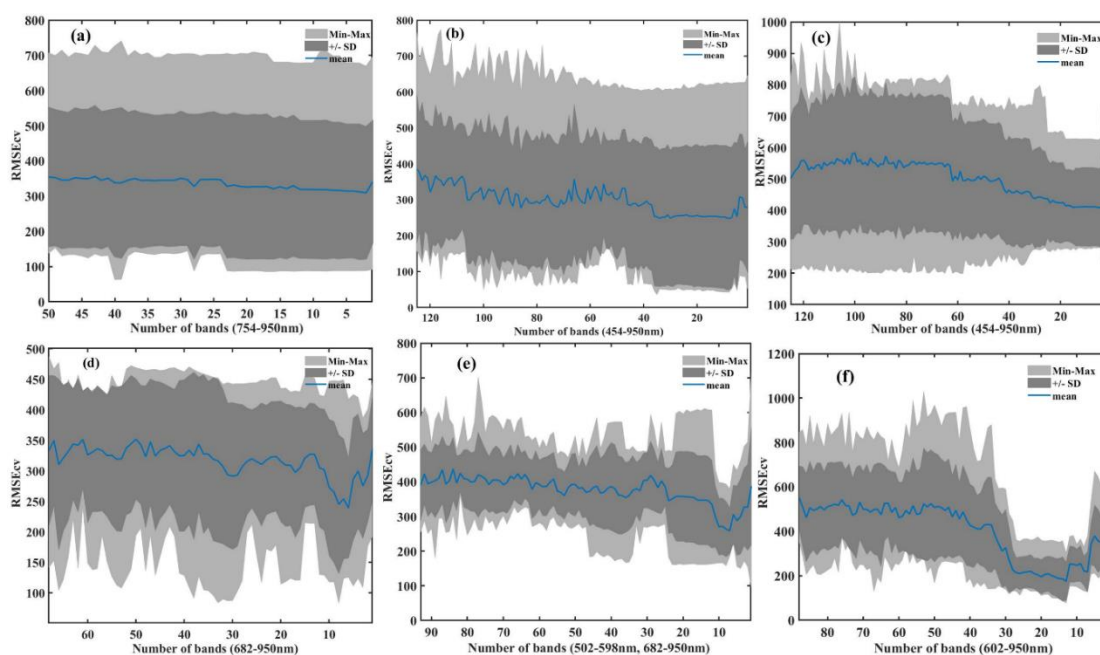| Growth Stages	Feature Types	Selected Spectra Features (nm)
BBCH-41	COS	778, 802, 950
	FDS	682, 718, 754, 762, 946, 950
BBCH-44	COS	742, 746, 750, 934, 938, 942
	FDS	558, 774, 798, 806, 862, 898, 950
BBCH-47	COS	570, 698, 702, 850
	FDS	610, 618, 642, 710, 722, 730, 758, 766, 850, 870, 922

Figure 4. Determination of COS and FDS spectral features for use in estimating potato AGB. Panels (**a**) and (**d**) show the cross-validation RMSEcv statistics (mean, standard deviation, and min–max ranges) obtained by applying the GPR-BAT to the COS and FDS, respectively, for the tuber-formation stage. Panels (**b**,**e**) show the same for the tuber-growth stage, and panels (**c**,**f**) show the same for the starch-storage stage.

To evaluate the reliability of potato AGB estimates based on canopy spectra, three machine-learning methods, SVM, RF, and GPR, were used to form potato AGB estimation models for the tuber-formation, tuber-growth, and starch-storage stages with the selected COS and FDS features. The values of R^2, RMSE, and NRMSE were used to evaluate the fit and stability of the models. The estimates obtained for each growth period are listed in Tables 4 and 5. The results show that the potato AGB of multiple growth periods cannot be accurately estimated based on the canopy spectral information. In addition, under the same conditions, AGB estimates made directly from the COS features (Table 4) are significantly less accurate than those made directly from the FDS features (Table 5). AGB estimates for the three potato growth stages made by using SVM, RF, and GPR, with the help of the canopy spectra COS and FDS, are most accurate for the tuber-growth period and degrade thereafter (Tables 4 and 5).

With COS as input, AGB estimates by the three machine-learning methods, SVM, RF, and GPR, for the tuber-growth period produced R^2 = 0.49, 0.55, and 0.58, respectively (SVM: RMSE = 299.97 kg/hm^2, NRMSE = 23.27%; RF: RMSE = 271.48 kg/hm^2, NRMSE = 21.06%; GPR: RMSE = 238.22 kg/hm^2, NRMSE = 18.48%). The AGB estimates with FDS as input produced R^2 = 0.56, 0.61, and 0.65, respectively (SVM: RMSE = 278.57 kg/hm^2, NRMSE = 21.61%; RF: RMSE = 242.09 kg/hm^2, NRMSE = 18.78%; GPR: RMSE = 223.92 kg/hm^2, NRMSE = 17.37%). The GPR method produced the highest R^2 for all three growth stages (COS: 0.42, 0.58, and 0.35; FDS: 0.58, 0.65, and 0.43) and the lowest RMSE (COS: 250.69, 238.22, and 341.41 kg/hm^2; FDS: 226.27, 223.92, and 326.32 kg/hm^2) and NRMSE (COS: 20.53%, 18.48%, and 23.53%; FDS: 18.53%, 17.37%, and 22.49%), indicating that the GPR method produces more accurate potato AGB estimates than the RF or SVM methods.

Table 4. Potato AGB estimates based on selected COS features using machine-learning methods for different growth stages.

Growth Stages	Methods	Modeling			Validation		
		R^2	RMSE (kg/hm^2)	NRMSE (%)	R^2	RMSE (kg/hm^2)	NRMSE (%)
BBCH-41	SVM	0.31	308.33	25.25	0.41	218.17	21.43
	RF	0.38	276.21	22.62	0.45	205.14	20.15
	GPR	0.42	250.69	20.53	0.56	187.52	18.42
BBCH-44	SVM	0.49	299.97	23.27	0.53	201.50	22.19
	RF	0.55	271.48	21.06	0.59	166.36	18.32
	GPR	0.58	238.22	18.48	0.61	148.38	16.34
BBCH-47	SVM	0.29	377.69	26.03	0.38	221.89	25.72
	RF	0.33	357.23	24.62	0.42	207.82	24.09
	GPR	0.35	341.41	23.53	0.53	193.51	22.43

Table 5. Potato AGB estimates based on selected FDS features using machine-learning methods for different growth periods.

Growth Stages	Methods	Modeling			Validation		
		R^2	RMSE (kg/hm^2)	NRMSE (%)	R^2	RMSE (kg/hm^2)	NRMSE (%)
BBCH-41	SVM	0.37	284.88	23.33	0.54	210.23	20.65
	RF	0.47	247.64	20.28	0.57	196.18	19.27
	GPR	0.58	226.27	18.53	0.61	175.61	17.25
BBCH-44	SVM	0.56	278.57	21.61	0.58	168.17	18.52
	RF	0.61	242.09	18.78	0.62	161.45	17.78
	GPR	0.65	223.92	17.37	0.68	143.65	15.82
BBCH-47	SVM	0.32	369.27	25.45	0.41	212.05	24.58
	RF	0.34	335.61	23.13	0.51	197.91	22.94
	GPR	0.43	326.32	22.49	0.58	185.92	21.55

3.3. Potato AGB Estimates Based on Vegetation Indices

Figure 5a shows the results of a Pearson correlation analysis between the selected VIs and potato AGB for multiple growth stages. The selected VIs correlate significantly with the AGB over the three growth stages ($p < 0.01$), with the correlation first increasing and then decreasing. The VI most strongly correlated with AGB during the tuber-formation stage is SPVI ($r = 0.672$, $p < 0.01$), and the VI most strongly correlated with AGB during both the tuber-growth and starch-storage stages is GNDVI ($r = 0.759$ and 0.756, respectively, $p < 0.01$). The scatter plots in Figure 5b,c reveal a linear correlation between the optimal VIs and AGB for each growth stage, although the sensitivity of the VIs to AGB decreases as the growth stage advances. The VIs saturate when the AGB is large. These results indicate that potato AGB estimates that use only a single VI are not reliable.
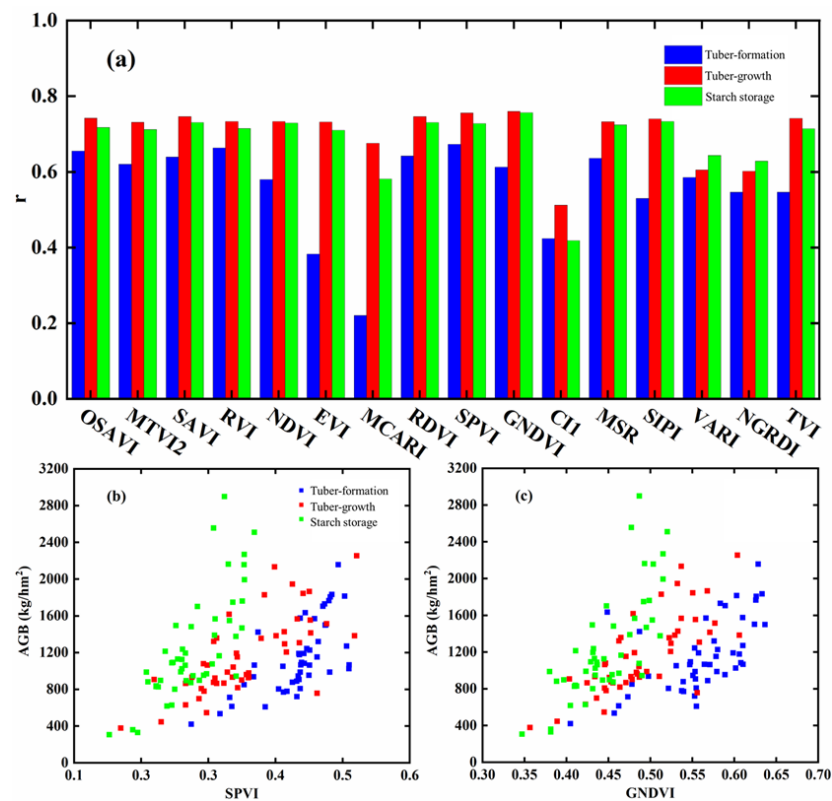
Figure 5. Pearson correlation analyses of above-ground biomass (AGB) of potatoes with VIs for different growth stages. (**a**) Absolute correlation coefficient for VIs versus AGB for tuber-formation, tuber-growth, and starch-storage periods. (**b**,**c**) Scatter plots of the best performing VIs versus AGB for each growth period.

Before constructing the potato AGB estimation model based on multiple VIs, we considered the autocorrelation of the independent input variables and used the "findcorrelation" function in the "caret" package of the R language to remove variables with high redundancy. The cutoff value of this function was set to 0.99. With the highly correlated independent variables removed, the remaining VIs used to estimate the AGB for each growth period are shown in Table 6. These are SAVI, NDVI, MSR, and TVI for all three potato growth stages, indicating that these Vis are essential for estimating the AGB.

Table 6. Remaining VIs after removing highly correlated variables for each growth stage.

Growth Stages	Selected Vegetation Indices
BBCH-41	OSAVI, SAVI, NDVI, MSR, NGRDI, TVI
BBCH-44	OSAVI, MTVI2, SAVI, NDVI, RDVI, SPVI, MSR, VARI, TVI
BBCH-47	MTVI2, SAVI, NDVI, RDVI, SPVI, MSR, NGRDI, TVI

The potato AGB during tuber-formation, tuber-growth, and starch-storage stages were estimated by using SVM, RF, and GPR with the selected VIs. The values of R^2, RMSE, and NRMSE for the regression results are given in Table 7. The results show that the AGB estimates become more accurate upon using the same machine-learning technique and VIs for each growth stage (Table 4, Table 5, and Table 7). The estimation accuracy peaks in the tuber-growth stage. Using the three machine-learning methods to estimate AGB for the tuber-growth stage produces R^2 = 0.59, 0.68, and 0.71 (SVM: RMSE = 266.90 kg/hm^2, NRMSE = 20.71%; RF: RMSE = 231.13 kg/hm^2, NRMSE = 17.93%; GPR: RMSE = 218.11 kg/hm^2, NRMSE = 16.92%). The largest R^2 value and the smallest RMSE and NRMSE values occur when using the GPR machine-learning method based on VIs, so this combination produced the best modeling results. However, the scatter plot (Figure 6)

shows that, during crop growth, potato AGB is underestimated when using VIs, regardless of the machine-learning method.

Table 7. Potato AGB estimates based on selected VIs for each growth stage.

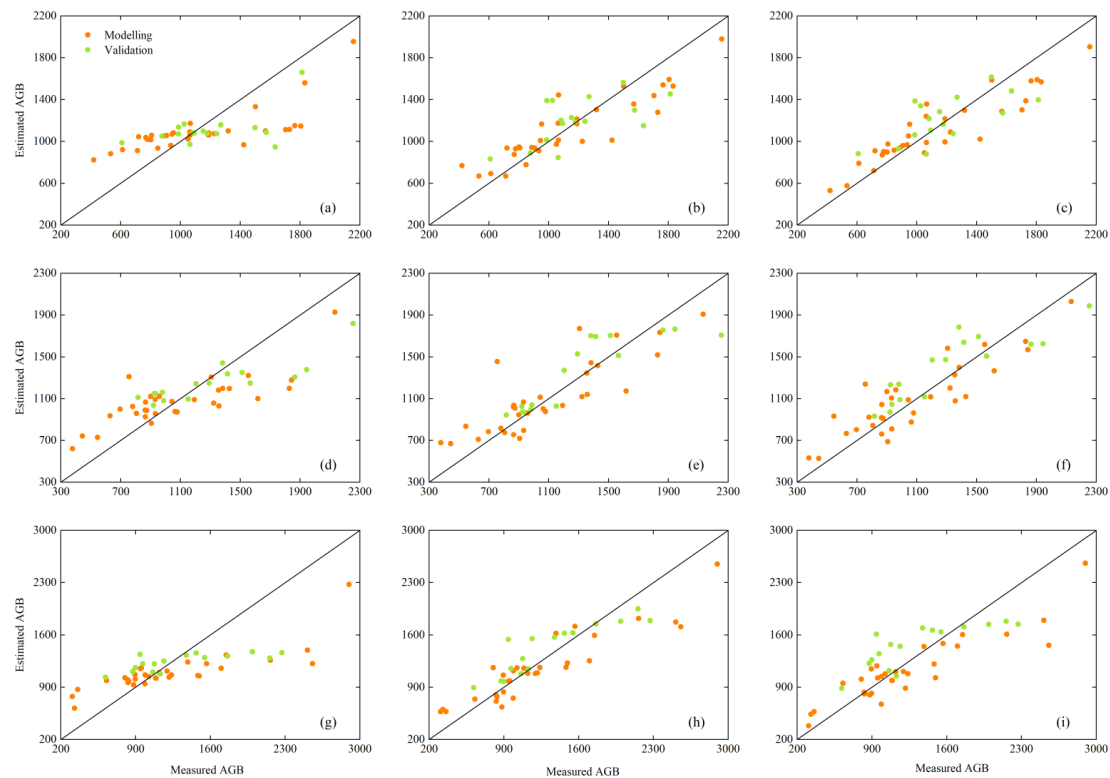| Growth Stages	Methods	Modeling			Validation		
		R^2	RMSE (kg/hm²)	NRMSE (%)	R^2	RMSE (kg/hm²)	NRMSE (%)
BBCH-41	SVM	0.45	270.47	22.15	0.61	205.44	20.18
	RF	0.62	243.61	19.95	0.65	174.70	17.16
	GPR	0.64	213.45	17.48	0.68	165.33	16.24
BBCH-44	SVM	0.59	266.90	20.71	0.63	163.63	18.02
	RF	0.68	231.13	17.93	0.72	139.57	15.37
	GPR	0.71	218.11	16.92	0.75	135.66	14.94
BBCH-47	SVM	0.43	356.21	24.55	0.58	205.93	23.87
	RF	0.53	329.66	22.72	0.62	184.79	21.42
	GPR	0.60	318.20	21.93	0.64	170.47	19.76

Figure 6. Scatter plots of measured versus estimated potato AGB (kg/hm²) for modeling and validation datasets and for different growth stages. SVM, RF, and GPR methods are used with VIs as input. (**a**–**c**) The relationship between measured and estimated potato AGB for the tuber-formation stage. Estimates were made by SVM, RF, and GPR, respectively. (**d**–**f**) Same as panels (**a**–**c**) but for the tuber-growth stage. (**g**–**i**) Same as panels (**a**–**c**) but for the starch-storage stage.

The validation dataset was used to verify the reliability of AGB estimates based on VIs combined with RF, SVM, or GPR for the three fertility stages of potato growth (Table 7 and Figure 6). The results show that the RF, SVM, and GPR methods were consistent across all growth stages. In other words, the fact that R^2, RMSE, and NRMSE follow the same trends for both the modeling and validation sets means that the models constructed by the three machine-learning methods fit the data well and are stable. Meanwhile, estimates based on VIs using the same machine-learning method were also consistent with the modeling set

and gradually improved when going from the tuber-formation stage to the tuber-growth stage, followed by deterioration. A comprehensive analysis, for each growth stage, of the accuracy metrics of the AGB estimation model (Table 7) revealed that the GPR method not only improves the accuracy but also enhances the stability, thereby providing the optimum AGB estimates and solving the saturation problem.

3.4. Estimation of Potato AGB Using Canopy Spectra and Vegetation Indices Combined with Crop Height

To evaluate how CH affects potato AGB estimates, the SVM, RF, and GPR machine-learning methods were used to develop AGB estimation models for the three growth stages by combining crop-canopy spectral information (COS, FDS), Vis, and CH. Before constructing the models, excessive redundancy between input parameters was avoided by using the "findCorrelation" function to exclude highly correlated independent variables. The final model factors for estimating potato AGB are listed in Table 8.

Table 8. Model factors involved after removing highly relevant variables for each growth stage.

Growth Stages	Selected Vegetation Indices
BBCH-41	718(FDS), NDVI, RDVI, SPVI, MSR, VARI, CH
BBCH-44	746(COS), 762(FDS), SAVI, EVI, RDVI, SPVI, MSR, SIPI, VARI, TVI, CH
BBCH-47	722(FDS), SAVI, NDVI, RDVI, SPVI, MSR, VARI, TVI, CH

AGB was estimated for each growth period by the three machine-learning methods (SVM, RF, and GPR) using the modeling dataset based on the model variables listed in Table 8. The regression results for R^2, RMSE, and NRMSE are listed in Table 9, and the fitted scatter plots are shown in Figure 7. The results show that the best estimates are obtained for each growth stage when estimating AGB by using the same machine-learning method with spectral information combined with CH (Table 4, Table 5, Table 7, and Table 9). The accuracy of the estimates produced by each machine-learning method vary from good to poor, peaking at the tuber-growth stage (Table 9). AGB estimates for the tuber-growth period using the three machine-learning methods produced R^2 = 0.64, 0.74, and 0.76, respectively (SVM: RMSE = 245.19 kg/hm^2, NRMSE = 19.02%; RF: RMSE = 223.79 kg/hm^2, NRMSE = 17.36%; GPR: RMSE = 199.68 kg/hm^2, NRMSE=15.49%).

Table 9. Potato AGB estimates based on spectral information combined with CH for each growth stage.

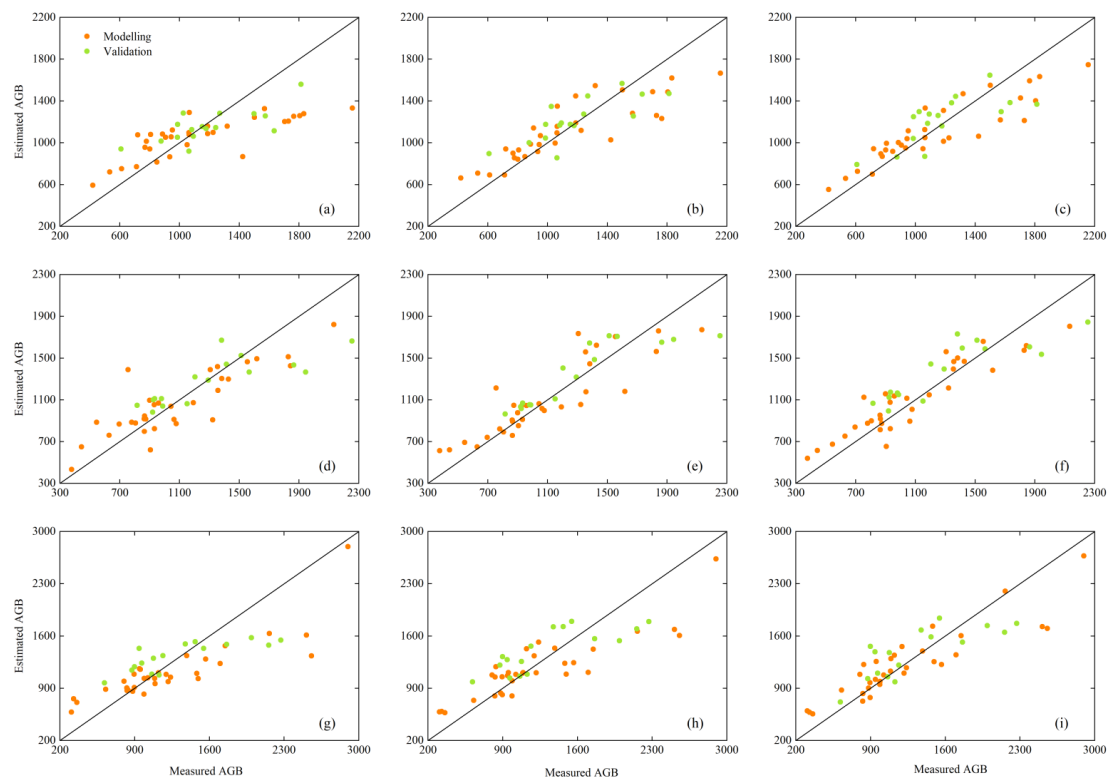| Growth Stages	Methods	Modeling			Validation		
		R^2	RMSE (kg/hm^2)	NRMSE (%)	R^2	RMSE (kg/hm^2)	NRMSE (%)
BBCH-41	SVM	0.58	263.39	21.57	0.66	196.38	19.29
	RF	0.69	228.71	18.73	0.75	172.35	16.93
	GPR	0.72	201.24	16.48	0.78	158.30	15.55
BBCH-44	SVM	0.64	245.19	19.02	0.69	168.17	18.52
	RF	0.74	223.79	17.36	0.79	141.84	15.62
	GPR	0.76	199.68	15.49	0.82	130.31	14.35
BBCH-47	SVM	0.56	334.59	23.06	0.62	198.25	22.98
	RF	0.62	310.80	21.42	0.65	176.94	20.51
	GPR	0.68	291.35	20.08	0.72	161.93	18.77

Figure 7. Scatter plots of measured versus estimated potato AGB (kg/hm^2) for modeling and validation datasets at different growth stages based on spectral information combined with CH and using SVM, RF, and GPR methods. (**a**–**c**) Relationship between measured and estimated potato AGB for the tuber-formation stage, as per SVM, RF, and GPR methods, respectively. (**d**–**f**) Same as panels (**a**–**c**) but for tuber-growth stage. (**g**–**i**) Same as panels (**a**–**c**) but for starch-storage stage.

The use of GPR fed with spectral information combined with CH improved the R^2 value and reduced the RMSE and NRMSE values, indicating that this method provides the most accurate estimate of potato AGB. At the same time, using any of the three machine-learning methods with the combination of CH and spectral information reduced the occurrence of AGB underestimation in each growth stage (Figures 6 and 7). Finally, the GPR method based on spectral information combined with CH handled the saturation problem of AGB estimation model better than the SVM and RF methods (Figure 7).

The stability of AGB estimation models constructed using SVM, RF, and GPR based on spectral information combined with CH was then verified by using the validation dataset. Figure 7 shows the relationship between the measured and estimated values for each potato growth stage. The results show that the SVM, RF, and GPR validation results are consistent with the modeling results for each fertility stage, and the higher the modeling accuracy, the higher the validation accuracy (Table 9), indicating that the models constructed by the three machine-learning methods are stable and that the prediction results are reliable. The prediction results obtained using the same machine-learning methods at each fertility stage were also consistent with the modeling dataset: a gradual improvement occurs upon going from tuber formation to tuber growth, following which deterioration sets in. In terms of model fit and stability, estimating potato AGB using the GPR method produced a higher R^2 and lower NRMSE, indicating that the GPR-AGB estimation method is more accurate than the SVM and RF methods.

4. Discussion

4.1. Monitoring Potato Crop Height

Variation in potato CH can provide researchers with important information on crop health, growth, and response to environmental impacts. Therefore, CH plays a decisive role

in monitoring crop growth [56–59], so CH data can not only guide agricultural production management but also provide a reliable theoretical basis for plant morphology research and crop selection and breeding. In this study, the CH information is extracted without generating a digital elevation model of bare-soil points by kriging interpolation because potatoes are planted in monopolies that reach a certain height, so ignoring their height and taking the difference would cause large extraction errors [60].

On the contrary, this study generates a high-density point cloud of UAV hyperspectral remote-sensing data by using structure-from-motion technology and then combining the location information of ground control points to generate a DSM for each fertility stage. Thus, the DSM for tuber-formation, tuber-growth, and starch-storage stages are differentially calculated from those of the bare-soil stage to obtain the CH of the corresponding fertility stage [61,62]. The relationship between extracted and measured CH is analyzed by using data from 144 samples from three fertility stages (Figure 2). The results give $R^2 = 0.84$ and NRMSE = 9.05%, indicating an accurate CH, which is consistent with the findings from Tao et al. [47], Bendig et al. [56,63], and Li et al. [49].

A comparative analysis reveals that the overall CH extracted in this study is small compared with the measured value, which is mainly because the UAV acquires hyperspectral data from the potato canopy, which has a tight spatial structure, so the spatial information from the top leaves may be removed as noise when performing three-dimensional point-cloud reconstruction. However, the measured CH is the height of the highest point of the leaves in the natural growth, which leads to an overall lower CH than the measured CH. At the same time, the images acquired by the UAV contain elements of potato-plant leaves and bare soil, so part of the soil affects the calculation of CH, which causes significant deviations. Therefore, the accuracy of three-dimensional point-cloud reconstruction of smaller structures in canopy space must be improved to accurately extract CH based on DSMs.

4.2. Estimation of Potato AGB Based on Canopy Spectra

How COS and FDS correlate with AGB must be analyzed before estimating potato AGB for the three reproductive stages. The results show that the correlations of both variables gradually increase upon going from the tuber-formation stage to the tuber-growth stage, following which they start to decrease. This result may be related to the potato crop growth cycle. Starting in the tuber-formation stage, the nutritional reproductive organs such as stems and leaves gradually develop, and the potato crop grows gradually and increases the vegetation cover. The spectral data are thus less affected by the ground soil when they are extracted. From the end of the tuber-growth stage to the beginning of the starch-storage stage, the organic matter created by above-ground photosynthesis is continuously transported to the underground tubers, robbing nutrients from the above-ground stems and leaves. At the same time, due to rainy weather, the plant leaves rapidly wither and fall off, causing the ground soil to seriously interfere with the extraction of spectral information from the crop canopy. The correlation between the FDS and AGB at this point is stronger than that for COS (Figure 3), which is consistent with the findings of Fan et al. [64] and Masjedi et al. [65] and is due to the ability to remove background noise and thereby enhance the spectral sensitivity by spectral differentiation [37]. Due to the numerous bands in the hyperspectral data, a serious collinearity problem exists between different spectral data. The GPR-BAT automatically identifies the characteristic bands in the sensitive spectral areas of the canopy (Figure 4) and determines the COS and FDS for estimating AGB at each growth stage (Table 3). More FDS features are screened in each growth period than are COS features, which indicates that the original spectrum contains more redundant information. The first-order derivative refines the spectral information and enhances the spectral sensitivity [63].

The SVM, RF, and GPR machine-learning methods are used to estimate AGB at each fertility stage based on the two spectral variables, COS and FDS, and the accuracy of each model is analyzed (Tables 4 and 5). The results show that, with the same machine-learning methods, the AGB estimates based on the two spectral variables progressively get more

accurate when going from the tuber-formation stage to the tuber-growth stage and then start to deteriorate, which may be closely related to potato growth. In addition, at each reproductive stage, AGB estimates based on FDS are better than those based on COS, which is consistent with the results of Feng et al. [65], indicating that the FDS better reflects the real AGB situation. However, comparing the estimation accuracy throughout the reproductive period shows that, although AGB may be estimated by using only crop-canopy spectral information (COS, FDS), the estimation accuracy is unsatisfactory (Tables 4 and 5).

4.3. Estimation of Potato AGB Based on Vegetation Indices

Based on previous studies, we selected 16 VIs that produce accurate AGB estimates (Table 1). These VIs correlated significantly with AGB ($p < 0.01$) across all fertility stages, with the correlations progressively increasing when going from the tuber-formation stage to the tuber-growth stage and then deteriorating. This result is consistent with the correlation of canopy spectral information with AGB (Figures 3 and 5). VIs are determined by the reflectance intensity in two or more spectral bands; however, the intensity of spectral reflectance has a limited response to variations in AGB [66]. As the growth stages advance, VIs tend to saturate (Figure 5), so estimating AGB by using a single VI is unreliable [37,44]. To reduce the autocorrelation between variables and improve efficiency, the model variables used to estimate AGB were obtained during each growth stage after excluding variables with high redundancy (Table 6). SAVI, NDVI, MSR, and TVI correlated strongly with AGB in each growth period, indicating that these indices contain important AGB information. This result is consistent with the findings of Gnyp et al. [8].

The SVM, RF, and GPR methods based on VIs were used to estimate the AGB at each growth stage (Table 5). The results show that AGB estimates using the same machine-learning method at each fertility stage are consistent with the variations based on canopy spectral information, which gradually improve upon going from tuber formation to tuber growth and then start to deteriorate. The models based on Vis (Table 7, Figure 6) were more accurate for each fertility period than those based on canopy spectral information (Tables 4 and 5), which is consistent with the results of Tao et al. [36]. In addition, differences appeared in the Vis used to estimate the three growth stages of potatoes, which is due to the different magnitude of variation in the AGB, leaf-area index, chlorophyll, and water content during crop growth. The VIs are related to these physicochemical parameters, making them sensitive to the AGB depending on the crop growth stage. Thus, the optimization of model-independent variables is vital for estimating the AGB based on UAV hyperspectral remote-sensing data.

4.4. Estimation of Potato AGB Based on Canopy Spectra, Vegetation Indices, and Crop Height

Estimating potato AGB using different machine-learning methods combined with crop-canopy spectral information (COS, FDS) and VIs is inaccurate because of crop spectral-response mechanisms (Table 4, Table 5, and Table 7 and Figure 6). Therefore, to overcome the saturation problem of the model and to estimate the AGB more accurately and across multiple fertility stages, the crop-canopy spectral information, Vis, and structural information (i.e., CH) are integrated to estimate potato AGB during the tuber-formation, tuber-growth, and starch-storage stages by using SVM, RF, and GPR. Before constructing the AGB estimation model for each fertility period, the final model variables used to estimate the AGB for each fertility period are obtained after excluding the variables with high autocorrelation (Table 8).

Model effects obtained using the same machine-learning method are consistent with the estimation effects based on canopy spectral information and Vis, which also gradually improve upon going from the tuber-formation to the tuber-growth stage, and then start to deteriorate. Comparing the model effects obtained when using the three variables at each fertility stage (Tables 4, 5, 7 and 8) shows that combining the extracted CH with canopy spectral information and Vis significantly improves the accuracy of AGB estimates and the stability of the model. This is consistent with the results of Banerjee et al. [23],

Zarco et al. [61], and Bendig et al. [62], who reported that the inclusion of CH information significantly improves the accuracy of AGB estimates. Using the three machine-learning methods based on spectral information and CH tends to underestimate the AGB less as the fertility stage progresses (Figures 6 and 7), indicating that CH is particularly important for monitoring potato AGB.

The R^2 values for AGB estimates produced by the SVM, RF, and GPR methods applied to the tuber-growth stage are 0.64, 0.74, and 0.76, respectively, and NRMSE = 19.02%, 17.36%, and 15.49%, respectively. Compared with the canopy-based original spectra, R^2 increases by 23%, 26%, and 24%, respectively, and NRMSE decreases by 22%, 21%, and 19%, respectively. Compared with the canopy-based first-derivative spectra, R^2 improves by 13%, 18%, and 14%, and NRMSE decreases by 14%, 8%, and 12%, respectively. Compared with VI-based estimates, R^2 improves by 7%, 8%, and 7%, and NRMSE decreases by 9%, 3%, and 9%, respectively. These results indicate that AGB estimates improve when using spectral information combined with CH.

4.5. Estimation of Potato AGB Using SVM, RF, and GPR Methods

SVM, RF, and GPR machine-learning methods were used to estimate AGB for each fertility stage based on different variables, with the results assessed by modeling and validating the dataset based on the magnitude of R^2, RMSE, and NRMSE. The results showed that the GPR method significantly improves the accuracy of potato AGB based on different types of variables (Tables 4, 5, 7 and 9, Figures 6 and 7). This indicates that the model constructed using the GPR method is superior, which is consistent with the results of Fu et al. [44], who estimated nitrogen indicators for winter wheat. This is mainly because, in the process of building the AGB estimation model with the GPR method, GPR-BAT automatically identifies important feature subsets related to potato AGB through the embedded feature-selection function, which not only reduces the complexity of the model but also improves its interpretability. At the same time, small datasets with nonlinear characteristics can be well-processed through the built-in kernel function, which makes the data fit better [44].

The AGB estimate at each fertility stage, produced by using the RF method based on different variables, is less accurate than that produced by the GPR method, mainly because the RF method is suitable for large datasets. The tuber-formation, tuber-growth, and starch-storage stages belong to the single-growth stage of potatoes with a small sample size (32 modeling data and 16 validation data qualify as small datasets), so AGB estimates produced by the RF method are not accurate.

However, using SVM to estimate AGB across all fertility stages and based on different variables is the least accurate, mainly because constructing the model with the SVM method is limited by penalty factors and kernel functions, which reduce the accuracy of AGB estimates. In addition, SVM depends on the collinearity of input variables. There may be some collinearity with the parameters involved in the final model construction in this study, resulting in the poor generalization of SVM to the data.

5. Conclusions

AGB plays an important role in monitoring crop growth, so the rapid and nondestructive acquisition of AGB data is vital for precision agriculture. Unlike satellite and aerial remote sensing, UAVs equipped with a UHD185 sensor can acquire potato crop-canopy images under cloud cover and can gather large amounts of spectral data with high spectral resolution, thereby providing a reliable technical support for crop AGB estimations. This study investigates the feasibility of using SVM, RF, and GPR methods based on COS, FDS, CH, Vis, and combinations thereof to estimate the potato AGB during tuber formation, tuber growth, and starch storage. The models constructed, based on different variables but using the same machine-learning method, all produce progressively more accurate AGB estimates when going from the tuber-formation stage to the tuber-growth stage, following which the accuracy deteriorates. The most accurate AGB estimates for each fertility

period are obtained by using the GPR method (independent of variables). Based on the combination of spectral information and CH, the SVM, RF, and GPR methods significantly improve the AGB estimation accuracy compared with the use of single-spectral features or VIs. However, the combination of spectral information and CH produces the most accurate AGB estimates and the most stable model, which is an important guideline for monitoring crop growth.

Author Contributions: H.F., Y.L., H.L., G.Y. and J.Y. designed the experiments. H.F., Y.F., Y.Z. and X.S. collected the AGB, CH, and UAV hyperspectral images. Y.L. and H.F. analyzed the data and wrote the manuscript. X.J. and J.Y. made comments and revised the manuscript. All authors have read and agreed to the published version of the manuscript.

Conflicts of Interest: The authors declare no conflict of interest.

References

1. Swain, K.C.; Thomson, S.J.; Jayasuriya, H.P. Adoption of an unmanned helicopter for low-altitude remote sensing to estimate yield and total biomass of a rice crop. *Trans. Asabe* **2010**, *53*, 21–27. [CrossRef]
2. Mueller, N.D.; Gerber, J.S.; Johnston, M.; Ray, D.K. Closing yield gaps through nutrient and water management. *Nature* **2013**, *494*, 254–261. [CrossRef]
3. Morier, T.; Cambouris, A.N.; Chokmani, K. In-season nitrogen status assessment and yield estimation using hyperspectral vegetation indices in a potato crop. *Agron. J.* **2015**, *107*, 1295–1309. [CrossRef]
4. Franceschini, M.D.; Harm, B.; Apeldoorn, D.; Suomalainen, J.; Kooistra, L. Intercomparison of unmanned aerial vehicle and ground-based narrow band spectrometers applied to crop trait monitoring in organic potato production. *Sensors* **2017**, *17*, 1428. [CrossRef]
5. Mahlein, A.K.; Rumpf, T.; Welke, P.; Dehne, H.W.; Plumer, L.; Steiner, U.; Oerke, E.C. Development of spectral indices for detecting and identifying plant diseases. *Remote Sens. Environ.* **2013**, *128*, 21–30. [CrossRef]
6. Greaves, H.E.; Vierling, L.A.; Eitel, J.H.; Boelman, N.T.; Magney, T.S.; Prager, C.M. Estimating aboveground biomass and leaf area of low stature arctic shrubs with terrestrial LiDAR. *Remote Sens. Environ.* **2015**, *164*, 26–35. [CrossRef]
7. Fu, Y.Y.; Yang, G.J.; Wang, J.H.; Song, X.Y.; Feng, H.K. Winter wheat biomass estimation based on spectral indices, band depth analysis and partial least squares regression using hyperspectral measurements. *Comput. Electron. Agric.* **2014**, *100*, 51–59. [CrossRef]
8. Gnyp, M.L.; Miao, Y.X.; Yuan, F.; Ustin, S.L.; Yu, K.; Yao, Y.K.; Huang, S.Y.; Bareth, G. Hyperspectral canopy sensing of paddy rice aboveground biomass at different growth stages. *Field Crop. Res.* **2014**, *155*, 42–55. [CrossRef]
9. Thenkabail, P.S.; Smith, R.B.; Pauw, E.D. Hyperspectral vegetation indices and their relationships with agricultural crop characteristics. *Remote Sens. Environ.* **2000**, *71*, 158–182. [CrossRef]
10. Angela, K.; Heather, M.; David, L.; Mark, S.; Catherine, C. Assessment of RapidEye vegetation indices for estimation of leaf area index and biomass in corn and soybean crops. *Int. J. Appl. Earth Obs.* **2015**, *34*, 235–248.
11. Asari, N.; Suratman, M.N.; Jaafar, J. Modelling and mapping of above ground biomass (AGB) of oil palm plantations in Malaysia using remotely-sensed data. *Int. J. Remote Sens.* **2017**, *38*, 4741–4764. [CrossRef]
12. Melian, J.M.; Jimenez, A.; Diaz, M.; Morales, A.; Horstrand, P.; Guerra, R.; Lopez, S. Real-time hyperspectral data transmission for UAV-based acquisition platform. *Remote Sens.* **2021**, *13*, 850. [CrossRef]
13. Yu, N.; Li, L.; Schmitz, N.; Tian, L.F.; Greenberg, J.A.; Diers, B.W. Development of methods to improve soybean yield estimation and predict plant maturity with an unmanned aerial vehicle-based platform. *Remote Sens. Environ.* **2016**, *187*, 91–101. [CrossRef]
14. Lydia, S.; Iolanda, F.; Josep, P. Remote sensing of biomass and yield of winter wheat under different nitrogen supplies. *Crop. Sci.* **2000**, *40*, 723–731.
15. David, A.J.; Hernan, D.B.; Jocelyn, C. Graph-based data fusion applied to: Change detection and biomass estimation in rice crops. *Remote Sens.* **2020**, *12*, 2683–2705.
16. Han, L.; Yang, G.; Dai, H.Y.; Xu, B.; Yang, H.; Feng, H.K.; Li, Z.H.; Yang, X.D. Modeling maize above-ground biomass based on machine learning approaches using UAV remote-sensing data. *Plant. Methods* **2019**, *15*, 10–24. [CrossRef]

17. Ma, B.L.; Dwyer, L.M.; Costa, C.; Cober, E.R.; Morrison, M.J. Early prediction of soybean yield from canopy reflectance measurements. *Agron. J.* **2001**, *93*, 1227–1234. [CrossRef]

18. Jan, C.; Lammert, K.; Marnix, V.B. Using sentinel-2 data for retrieving LAI and Leaf and canopy chlorophyll content of a potato crop. *Remote Sens.* **2017**, *9*, 405–427.

19. Gitelson, A.A.; Vian, A.; Arkebauer, T.J.; Rundquist, D.C.; Keydan, G.; Leavitt, B. Remote estimation of leaf area index and green leaf biomass in maize canopies. *Geophys. Res. Lett.* **2003**, *30*, 1248–1270. [CrossRef]

20. Kanemasu, E.T. Seasonal canopy reflectance patterns of wheat, sorghum, and soybean. *Remote Sens. Environ.* **1974**, *3*, 43–47. [CrossRef]

21. Kooistra, L.; Clevers, J.W. Estimating potato leaf chlorophyll content using ratio vegetation indices. *Remote Sens. Lett.* **2016**, *7*, 611–620. [CrossRef]

22. Daughtry, C.T.; Walthall, C.L.; Kim, M.S.; Colstoun, E.B.; Mcmurtrey, J.E. Estimating corn leaf chlorophyll concentration from leaf and canopy reflectance. *Remote Sens. Environ.* **2000**, *74*, 229–239. [CrossRef]

23. Banerjee, B.P.; Spangenberg, G.; Kant, S. Fusion of spectral and structural information from aerial images for improved biomass estimation. *Remote Sens.* **2020**, *12*, 3164. [CrossRef]

24. Monica, H.; Pablo, R.G.; Katy, M.R. Yield prediction by machine learning from UAS-based multi-sensor data fusion in soybean. *Plant. Methods* **2020**, *16*, 78–91.

25. Guo, A.T.; Huang, W.J.; Dong, Y.Y.; Ye, H.C.; Ma, H.Q.; Liu, B. Wheat yellow rust detection using UAV-based hyperspectral technology. *Remote Sens.* **2021**, *13*, 123. [CrossRef]

26. Eweys, O.A.; Elwan, A.A.; Borham, T.I. Integrating WOFOST and Noah LSM for modeling maize production and soil moisture with sensitivity analysis, in the east of The Netherlands. *Field Crop. Res.* **2017**, *210*, 147–161. [CrossRef]

27. Zhou, G.X.; Liu, X.N.; Liu, M. Assimilating remote sensing phenological information into the WOFOST model for rice growth simulation. *Remote Sens.* **2019**, *11*, 268. [CrossRef]

28. Onisimo, M.; Elhadi, A.; Moses, A.C. High density biomass estimation for wetland vegetation using WorldView-2 imagery and random forest regression algorithm. *Int. J. Appl. Earth Obs.* **2012**, *18*, 399–406.

29. Hansen, P.M.; Schjoerring, J.K. Reflectance measurement of canopy biomass and nitrogen status in wheat crops using normalized difference vegetation indices and partial least squares regression. *Remote Sens. Environ.* **2003**, *86*, 542–553. [CrossRef]

30. Behmann, J.; Mahlein, A.K.; Rumpf, T.; Romer, C.; Plumer, L. A review of advanced machine learning methods for the detection of biotic stress in precision crop protection. *Precis. Agric.* **2015**, *16*, 239–260. [CrossRef]

31. Andres, V.; Gitelson, A.A.; Nguy-Robertson, A.L.; Peng, Y. Comparison of different vegetation indices for the remote assessment of green leaf area index of crops. *Remote Sens. Environ.* **2011**, *115*, 3468–3478.

32. Yue, J.B.; Yang, G.J.; Tian, Q.J.; Feng, H.K.; Xu, K.J.; Zhou, C.Q. Estimate of winter-wheat above-ground biomass based on UAV ultrahigh-ground-resolution image textures and vegetation indices. *ISPRS J. Photogramm.* **2019**, *150*, 226–244. [CrossRef]

33. Jia, M.; Li, W.; Wang, K.; Zhou, C.; Cheng, T.; Tian, Y.; Zhu, Y.; Cao, W. A newly developed method to extract the optimal hyperspectral feature for monitoring leaf biomass in wheat. *Comput. Electron. Agric.* **2019**, *165*, 104942. [CrossRef]

34. Jin, X.L.; Yang, G.J.; Xu, X.G.; Yang, H.; Feng, H.K.; Li, Z.K.; Zhao, C.J. Combined multi-temporal optical and radar parameters for estimating LAI and biomass in winter wheat Using HJ and RADARSAR-2 Data. *Remote Sens.* **2015**, *7*, 13251. [CrossRef]

35. Liu, Y.; Feng, H.K.; Yue, J.B.; Li, Z.H.; Yang, G.J.; Song, X.Y.; Yang, X.D. Remote-sensing estimation of potato above-ground biomass based on spectral and spatial features extracted from high-definition digital camera images. *Comput. Electron. Agric.* **2022**, *198*, 107089. [CrossRef]

36. Tao, H.L.; Feng, H.K.; Xu, L.J.; Miao, M.K.; Long, H.L.; Yue, J.B. Estimation of crop growth parameters using UAV-based hyperspectral remote sensing data. *Sensors* **2020**, *20*, 1296. [CrossRef] [PubMed]

37. Yue, J.B.; Feng, H.K.; Yang, G.J.; Li, Z.H. A Comparison of regression techniques for estimation of above-ground winter wheat biomass using near-surface spectroscopy. *Remote Sens.* **2018**, *10*, 66. [CrossRef]

38. Pugh, N.A.; Horne, D.W.; Murray, S.C.; Carvalho, G.; Malambo, L.; Jung, J.H. A Temporal estimates of crop growth in sorghum and maize breeding enabled by unmanned aerial systems. *Plant. Phenome J.* **2017**, *28*, 170006. [CrossRef]

39. Varela, S.; Assefa, Y.; Prasad, P.V.; Peralta, N.R.; Griffin, T.W.; Sharda, A.; Ferguson, A. Spatio-temporal evaluation of plant height in corn via unmanned aerial systems. *J. Appl. Remote Sens.* **2017**, *11*, 12–32. [CrossRef]

40. Muharam, F.M.; Bronson, K.F.; Maas, S.J.; Ritchie, G.L. Inter-relationships of cotton plant height, canopy width, ground cover and plant nitrogen status indicators. *Field Crop. Res.* **2014**, *169*, 58–69. [CrossRef]

41. Fenner, H.; Andrew, R.; Adam, M.; Wooster, M.J.; Hawkesford, M.J. High throughput field phenotyping of wheat plant height and growth rate in field plot trials using UAV based remote sensing. *Remote Sens.* **2016**, *8*, 1031.

42. Zheng, B.H.; Zhang, L.; Xie, D.; Yin, X.L.; Liu, C.J.; Liu, G. Application of synthetic NDVI time series blended from Landsat and MODIS data for grassland biomass estimation. *Remote Sens.* **2016**, *8*, 10. [CrossRef]

43. Wang, L.A.; Zhou, X.D.; Zhu, X.K.; Dong, Z.D.; Guo, W.S. Estimation of biomass in wheat using random forest regression algorithm and remote sensing data. *Crop. J.* **2016**, *4*, 212–219. [CrossRef]

44. Fu, Y.Y.; Yang, G.J.; Li, Z.H.; Song, X.Y.; Li, Z.H.; Xu, X.G.; Wang, P.; Zhao, C.J. Winter wheat nitrogen status estimation using UAVbased RGB imagery and gaussian processes regression. *Remote Sens.* **2020**, *12*, 3778. [CrossRef]

45. Verrelst, J.; Alonso, L.; Camps-Valls, G.; Delegido, J.; Moreno, J. Retrieval of vegetation biophysical parameters using gaussian process techniques. *IEEE Trans. Geosci. Remote. Sens.* **2012**, *50*, 1832–1843. [CrossRef]

46. Rondeaux, G.; Steven, M.; Baret, F. Optimization of soil-adjusted vegetation indices. *Remote Sens. Environ.* **1996**, *55*, 95–107. [CrossRef]

47. Tao, H.L.; Feng, H.K.; Xu, L.J.; Miao, M.K.; Yang, G.J. Estimation of the yield and plant height of winter wheat using uav-based hyperspectral images. *Sensors* **2020**, *20*, 1231. [CrossRef]

48. Zheng, H.; Cheng, T.; Zhou, M.; Li, D.; Yao, X. Improved estimation of rice aboveground biomass combining textural and spectral analysis of UAV imagery. *Precis. Agric.* **2018**, *20*, 611–629. [CrossRef]

49. Wu, C.; Niu, Z.; Tang, Q.; Huang, W. Estimating chlorophyll content from hyperspectral vegetation indices: Modeling and validation. *Agric. For. Meteorol.* **2008**, *148*, 1230–1241. [CrossRef]

50. Li, B.; Xu, X.; Zhang, L.; Han, J.; Bian, C. Above-ground biomass estimation and yield prediction in potato by using UAV-based RGB and hyperspectral imaging. *ISPRS J. Photogramm.* **2020**, *162*, 161–172. [CrossRef]

51. Broge, N.H.; Leblanc, E. Comparing prediction power and stability of broadband and hyperspectral vegetation indices for estimation of green leaf area index and canopy chlorophyll density. *Remote Sens. Environ.* **2001**, *76*, 156–172. [CrossRef]

52. Gitelson, A.A.; Kaufman, Y.J.; Stark, R.; Rundquist, D. Novel algorithms for remote estimation of vegetation fraction. *Remote Sens. Environ.* **2002**, *80*, 76–87. [CrossRef]

53. Prasad, A.M.; Iverson, L.R.; Liaw, A. Newer classification and regression tree techniques: Bagging and random forests for ecological prediction. *Ecosystems* **2006**, *9*, 181–199. [CrossRef]

54. Gleason, C.J.; Junho, I. Forest biomass estimation from airborne LiDAR data using machine learning approaches. *Remote Sens. Environ.* **2012**, *125*, 80–91. [CrossRef]

55. Verrelst, J.; Rivera, J.P.; Gitelson, A.; Delegido, J.; Moreno, J.; Camps-Valls, G. Spectral band selection for vegetation properties retrieval using Gaussian processes regression. *Int. J. Appl. Earth Obs.* **2016**, *52*, 554–567. [CrossRef]

56. Bendig, J.; Bolten, A.; Bennertz, S.; Broscheit, J.; Bareth, G. Estimating biomass of barley using crop surface models (CSMs) derived from UAV-based RGB imaging. *Remote Sens.* **2014**, *6*, 10395. [CrossRef]

57. Brocks, S.; Bareth, G. Estimating barley biomass with crop surface models from oblique RGB imagery. *Remote Sens.* **2018**, *10*, 268. [CrossRef]

58. Souza, C.D.; Lamparelli, R.C.; Rocha, J.V. Height estimation of sugarcane using an unmanned aerial system (UAS) based on structure from motion (SfM) point clouds. *Int. J. Remote Sens.* **2017**, *38*, 2218–2273. [CrossRef]

59. Ballesteros, R.; Ortega, J.F.; Hernandez, D.; Moreno, M.A. Onion biomass monitoring using UAV-based RGB imaging. *Precis. Agric.* **2018**, *19*, 840–857. [CrossRef]

60. Liu, Y.; Feng, H.K.; Huang, J.; Sun, Q.; Yang, F.Q. Estimation of potato biomass based on UAV digital images. *Trans. Chin. Soc. Agric. Eng.* **2020**, *36*, 182–192.

61. Zarco, P.J.; Diza, R.; Angileri, V.; Loudjani, P. Tree height quantification using very high resolution imagery acquired from an unmanned aerial vehicle (UAV) and automatic 3D photo-reconstruction methods. *Eur. J. Agron.* **2014**, *55*, 89–99. [CrossRef]

62. Bendig, J.; Bolten, A.; Bareth, G. UAV-based imaging for multi-temporal, very high resolution crop surface models to monitor crop growth variability. *Photogramm. Fernerkund. Geoinf.* **2013**, *6*, 551–562. [CrossRef]

63. Fan, L.L.; Zhao, J.L.; Xu, X.G.; Liang, D.; Yang, G.J.; Feng, H.K. Hyperspectral-based estimation of leaf nitrogen content in corn using optimal selection of multiple spectral variables. *Sensors* **2019**, *19*, 2898. [CrossRef] [PubMed]

64. Masjedi, A.; Crawford, M.M.; Carpenter, N.R.; Tuinstra, M.R. Multi-Temporal predictive modelling of sorghum biomass using UAV-based hyperspectral and LiDAR data. *Remote Sens.* **2020**, *12*, 3587. [CrossRef]

65. Feng, W.; Guo, B.B.; Zhang, H.Y.; He, L.; Zhang, Y.S.; Wang, Y.H.; Zhu, Y.J.; Guo, T.C. Remote estimation of above ground nitrogen uptake during vegetative growth in winter wheat using hyperspectral red-edge ratio data. *Field Crop. Res.* **2015**, *180*, 197–206. [CrossRef]

66. Oppelt, N.; Mauser, W. Hyperspectral monitoring of physiological parameters of wheat during a vegetation period using AVIS data. *Int. J. Remote Sens.* **2004**, *25*, 145–159. [CrossRef]